

Locating Acoustic Emission Signals Due to Shock Impacts on a Carbon Fiber Sample Using Piezoelectric and Fiber Optic Sensors

L. N. Stepanova^{a,*,**}, S. I. Kabanov^{a,**}, and V. V. Chernova^{b,**}

^a Chaplygin Siberian Research Institute of Aviation, Novosibirsk, 630051 Russia

^b Siberian Transport University, Novosibirsk, 630049 Russia

*e-mail: aergru@ngs.ru

**e-mail: stepanova@stu.ru

Received February 18, 2022; revised March 9, 2022; accepted March 11, 2022

Abstract—Comparative tests related to locating acoustic emission (AE) signals due to shock impacts on a T700 carbon fiber sample were carried out. Piezoelectric acoustic emission transducers (AETs) and fiber-optic sensors (FOSs) were installed on the sample, forming rectangular location antennas measuring 360 × 280 mm. Strikes were delivered with balls weighing 10 and 18.5 g. Antennas consisting of four AET sensors and four FOS sensors and an antenna consisting of two AET sensors and two FOS sensors were organized. When using the antenna containing four FOS sensors, the impact on the sample was produced by a load weighing 530 g dropped from a height of 400 mm. AE signals were recorded by the SCAD-16.10 system with “floating” selection thresholds when the ball was dropped and during its repeated bounces. Then AE signal clusters were formed and recorded during the impact of loads. The arrival times of AE signals to the antenna sensors were calculated using the threshold method, the root mean square (RMS) deviation method and the two-interval method. It is shown that the maximum error in locating AE signals is observed when a steel ball with a diameter of 16 mm is dropped from a height of 300 mm and the minimum error is when using an electronic simulator.

Keywords: carbon fiber, static, shock, defect, acoustic emission, location, error, piezoelectric and fiber optic sensors

DOI: 10.1134/S106183092204009X

INTRODUCTION

In the process of loading aircraft structures made of composite materials (CMs), the effects of shock damage, overloads causing their stratification, and deterioration of strength and stiffness characteristics are investigated. The resulting defects can lead to sudden destruction of the carbon fiber material. The danger is represented even by relatively small impacts that do not leave visible marks on the surface of the composite structure but produce internal defects [1–3].

Monitoring and evaluating the development of defects due to impacts in the elements of aircraft structures made of carbon fiber requires both recording the collision process and the subsequent testing of the material in the impact area [4, 5].

Ultrasonic, X-ray, thermal imaging, optical, acoustic emission (AE), and other methods of nondestructive testing (NDT) are used to inspect composite material structures. The AE method has high sensitivity and allows one to determine defect hazardousness, localize destruction zone in real time, and assess the residual life of the structure.

When testing carbon fiber structures, it is necessary to take into account the effect of anisotropy on the propagation velocity of elastic waves from defects, which affects the accuracy of their location. The presence of noise from loading devices, difficulties in obtaining live data about the main informative parameters of AE signals that are related functionally to the processes of defect development and structural failure—all this requires further analysis and development of testing methods to improve accuracy.

In the results of AE studies by NASA, it was noted that when registering impacts in aerospace structures, the microstructure of the composite affects not only its strength and mechanical properties but also the structure of the AE signals themselves [6]. When solving problems of locating defects, this can degrade

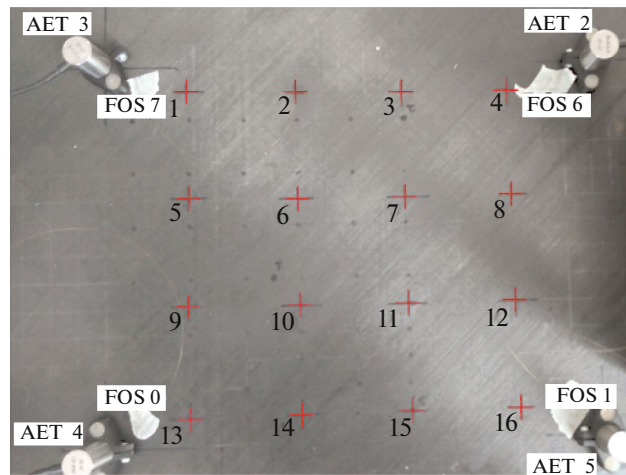


Fig. 1. Appearance of location antenna with piezoelectric and fiber-optic sensors and marked impact sites on a carbon fiber sample.

accuracy and complicate the decoding and processing of AE information. Informative parameters such as MARSE, structural coefficient, planar location, impact energy, and amplitude distribution are used [7–11] when developing testing methods for determining the coordinates, type, and hazardousness of a defect in composite structures.

It is known that AE systems mainly work with piezoelectric acoustic emission transducers (AET). However, at present, both in our country [8, 12–14] and abroad [15–20], research is being carried out in which fiber-optic sensors (FOS) are included in antennas used in AE testing. One of the main advantages of FOS sensors (compared to AET sensors) worth mentioning are small dimensions and weight, insensitivity to electromagnetic noise and interference, weak sensitivity to vibration, linearity of the amplitude-frequency response, the ability to use a single optical fiber for multipoint measurements, and the organization of various types of sensors on a single fiber designed not only to work with acoustic signals but also for measuring temperature and strain [12].

The aim of this work is to analyze the results of locating AE signals recorded in a carbon fiber sample from shock loads using an AE system operating with various antennas consisting of a combination of piezoelectric and fiber optic sensors.

RESEARCH PROCEDURE

For the tests, we used a T700 carbon fiber sample with a size of $800 \times 450 \times 1.2$ mm, where four piezoelectric sensors PC 01-07 and four Fabry–Perot FOS sensors were installed to form rectangular location antennas with dimensions of 360×280 mm (Fig. 1). Four types of antennas were organized when recording AE information during shock loading of the sample. The first antenna consisted of four piezoelectric AET sensors. The second and third antennas consisted of two piezoelectric AET sensors and two FOS sensors. Four FOS sensors were included in the fourth antenna. Errors in locating AE signals during load discharge and rebound were determined in the tests.

Prior to testing, 16 points spaced 80 mm from each other were marked in the working area of the sample (see Fig. 1). First, we used the first antenna, consisting of four piezoelectric AET sensors operating in the frequency range 100–700 kHz. Recording of AE information was carried out by an SCAD-16.10 AE system with “floating” selection thresholds (certificate of the Federal Agency for Technical Regulation and Metrology RU.C.27/007 A no. 40707, registration number in the State Register of Measuring Instruments 45154-10).

Errors in measuring the coordinates of defects in composite structures determined by the AE method depend on errors in measuring the arrival time of signals to antenna sensors and on errors in determining the sonic speed in the working area [4, 5]. To measure the speed of sound in T700 carbon fiber, automated calibration of the working location zone of the sample was carried out in which each AET sensor was alternately switched to the emission mode, with the remaining three antenna sensors operating in the reception mode.

According to calibration results, the sound velocity of the fast mode S_0 propagating in the direction of the X -axis between sensors AET4 and AET5 (see Fig. 1) was $V_x = 360 \text{ mm}/72 \mu\text{s} = 5.0 \text{ mm}/\mu\text{s}$. The propagation velocity of the fast mode S_0 passing along the Y -axis from sensor AET4 to sensor AET3 was equal to $V_y = 280 \text{ mm}/48 \mu\text{s} = 5.83 \text{ mm}/\mu\text{s}$ and that in the XY -direction from sensor AET4 to sensor AET2, $V_{xy} = 456 \text{ mm}/84 \mu\text{s} = 5.43 \text{ mm}/\mu\text{s}$. Thus, an appreciable anisotropy was observed for this sample in terms of the speed of sound. Based on the results of automated calibration, the coordinates of the AET sensors in the location zone were determined in units of time (μs) for the fast mode S_0 : AET4 (0; 0), AET5 (72.7; 0); AET2 (72.7; 48.5); and AET3 (0; 48.5).

Before the start of impact tests, signals from a simulator were introduced at each of the 16 points marked on the sample (see Fig. 1). Two types of simulators were used. When working with the Su–Nielsen simulator, a 0.5 mm diameter pencil lead with a hardness of 2H was fractured at an angle of 45° at each point. When working with an electronic simulator, electrical signals with a voltage of 80 V and a duration of 150 μs were introduced at each point. The signal from the electronic simulator was transmitted to the piezoelectric AET sensor and switched the sensor into emission mode. After experiments with the simulators, errors in determining the coordinates of each point marked on the sample were calculated.

Then the impacts associated with dropping steel balls from a height of $h_1 = 300 \text{ mm}$ and $h_2 = 600 \text{ mm}$ into each point marked on the sample were performed. Balls with a diameter of $d_1 = 10 \text{ mm}$ and a weight of 4.5 g and with a diameter of $d_2 = 16 \text{ mm}$ and a weight of 18.5 g were used for testing. The precise discharge of the balls at each point on the sample was achieved through using a 600 mm long pipe. The ball with the diameter of $d_2 = 16 \text{ mm}$ was dropped from a height of $h_1 = 300 \text{ mm}$ and the ball with the diameter of $d_2 = 10 \text{ mm}$ was dropped from a height of $h_2 = 600 \text{ mm}$.

The impact energy was determined as [10]

$$E = mgh, \quad (1)$$

where m is the load mass, kg, g is the acceleration due to gravity, m/s^2 , and h is the load drop height, m.

Thus, the energy of the ball with mass $m_1 = 4.5 \text{ g}$ dropped from the height of $h_2 = 600 \text{ mm}$ determined by formula (1) amounted to $E_{12} = 0.026 \text{ J}$. The impact energy when dropping the ball with mass $m_2 = 18.5 \text{ g}$ from the height of $h_1 = 300 \text{ mm}$ was $E_{21} = 0.055 \text{ J}$.

AE signals were recorded by the system both after the ball was dropped and during its repeated bounces. Then clusters of AE signals recorded during shock impacts at each point of the sample were formed [21]; 16 clusters were formed and for each of them the coordinates of the center were determined as the average value of the coordinates of all signals in the cluster. To determine the coordinates of the points marked on the sample, the location of the AE signals was carried out. The random component of the coordinate error was calculated from the root mean square deviations (S_{xi}, S_{yi}) in each cluster [22].

In the calculation, the systematic component of the error in the X - and Y -coordinates of the cluster center was determined in units of the arrival time difference (ATD) in microseconds and multiplied by the speed of the fast mode S_0 along the X (5.0 $\text{mm}/\mu\text{s}$) and Y (5.83 $\text{mm}/\mu\text{s}$) axes. The coordinates of the location center were determined in millimeters as [22]

$$X_i = x_{\text{ATD}} V_x; \quad Y_i = y_{\text{ATD}} V_y,$$

where i is the number of the impact point (cluster), x_{ATD} and y_{ATD} are the coordinates of the sensors in the time domain, μs ; X_i and Y_i are the measured coordinates of the source along the X - and Y -axes, mm, and V_x and V_y are the propagation velocities of the fast mode S_0 along the X - and Y -axes, $\text{mm}/\mu\text{s}$.

Calculations were carried out using the threshold method, the root mean square deviation method, and the two-interval method [7, 10] to determine the errors in the arrival times of AE signals to AET sensors.

The arrival time according to the threshold method was calculated by the moment when an AE signal exceeds a certain level determined by noise in its past history. At the same time, automatic detection of the threshold level was introduced, where the threshold was set as [7]

$$U_{\text{thr}} = U_{\text{noise}} + U_{\text{add noise}},$$

where U_{noise} is the noise level calculated in the area of the signal past history and $U_{\text{add noise}}$ is an addition to the noise level.

When using the RMS deviation method, we used a time “window” of several microseconds superimposed on the digitization of the AE signal. In the “window,” we calculated a certain parameter responding

to a local change in the signal structure. This algorithm considerably increases the degree of reliability of determining the arrival times of AE signals compared to the method based on threshold discrimination [7]. When moving the “window” on digitization, the RMS deviation parameter was chosen for the signal structure parameter characterizing the energy level [7, 9],

$$\sigma_j = \sqrt{\frac{\sum_{i=T_1}^{i=T_2} (x_i - x_{\text{avg}})^2}{T_2 - T_1 - 1}},$$

where T_1 and T_2 are the numbers of the counts by the analog-to-digital converter corresponding to the moments of the beginning and end of the time “window,” x_{avg} is the average value of the AE signal realization in the “window,” and i is the number of the point in the RMS array.

The advantage of this method is manifested in processing complex multimode signals, when several acoustic wave modes are present in the digitization. By selecting the threshold level, it is possible to tune in to determine the beginning of the signal in the selected mode [7].

The two-interval method allows one to determine the time of arrival of the AE signal, coinciding with the moment of a change in its power. The structure parameter $A(t)$ of the AE signal is written as [7]

$$A(t) = \int_t^{t+T_{\text{window}}} |U(t)| dt,$$

where $U(t)$ is the AE electrical signal and T_{window} is the size of the “window” used for calculating the signal power.

The arrival time of the AE signal corresponds to the maximum value of the modified two-interval coefficient $K(t)$ defined [8] as

$$K(t) = \frac{A(t + T_{\text{window}}) - A(t - T_{\text{window}})}{A(t - T_{\text{window}})}.$$

The advantage of using the two-interval method is that summing the parameters of the AE signal structure in a time “window” practically eliminates random outliers. This makes it possible to more accurately determine the arrival time t_0 of the AE signal to the corresponding AET sensor, and, consequently, to reduce the spread of the defect coordinates and determine them automatically [8].

The design random error components for each impact point (see Fig. 1) were determined using the formulas [10, 22]

$$S_{xi} = \sqrt{\frac{\sum_{i=1}^n (x_i - x_{\text{avg}})^2}{(n-1)}}; \quad S_{yi} = \sqrt{\frac{\sum_{i=1}^n (y_i - y_{\text{avg}})^2}{(n-1)}},$$

where n is the number of counts, x_i and y_i are the measured values along the X - and Y -axes, and x_{avg} and y_{avg} are the average values along the X - and Y -axes.

The resulting random error S_{xyi} for each point of the sample is [22]

$$S_{xyi} = \sqrt{(S_{xi}^2 + S_{yi}^2)},$$

where S_{xi} and S_{yi} are the calculated coordinates along the X - and Y -axes, mm.

The systematic component of the error for each coordinate was estimated as the modulus of the difference between the coordinates of the cluster center (X_i, Y_i) and the coordinates X_{i0} and Y_{i0} measured by a gaged ruler,

$$\Delta X_i = |X_i - X_{i0}|;$$

$$\Delta Y_i = |Y_i - Y_{i0}|,$$

where i is the number of the impact point (cluster) and X_i and Y_i are the measured coordinates of the source, mm.

Table 1. Systematic and random location errors for various methods of calculating ATD when using antenna consisting of four AETs

ATD calculation method	$S1$, mm	$\Delta 1$, mm	$S2$, mm	$\Delta 2$, mm	$S3$, mm	$\Delta 3$, mm
RMSD	1.8	5.4	3.5	6.1	7.7	10.2
	1.0%	7.7%	2.5%	5.7%	2.4%	7.7%
Threshold	1.7	5.4	4.3	6.1	23.4	22.0
	0.6%	1.9%	1.6%	2.2%	8.4%	7.9%
Two-interval	7.2	6.7	9.4	7.9	23.9	15.6
	2.6%	2.4%	3.0%	2.7%	8.6%	5.6%

The total systematic error at each point of the sample was determined by the formula [22]

$$\Delta XY_i = \sqrt{(\Delta X_i^2 + \Delta Y_i^2)},$$

where ΔX_i and ΔY_i are the calculated systematic components of the error along the X - and Y -axes, mm.

RESULTS AND DISCUSSION

The systematic and random components of the error in calculating the coordinates of the location of AE signals when using the antenna consisting of four AETs were averaged over all impact points. The calculation results are listed in Table 1, where $S1$ and $\Delta 1$ indicate random and systematic errors obtained when determining the coordinates of the location zone using electronic simulator; $S2$ and $\Delta 2$, when dropping the metal ball with diameter $d = 10$ mm from height $h = 600$ mm; and $S3$ and $\Delta 3$, when dropping the metal ball with diameter $d = 16$ mm from height $h = 300$ mm.

The arrival times of AE signals for the fast mode $S0$ were determined by the RMSD method [7]. Then, the values of the coordinates of the signal source in ATD units were calculated using triangulation formulas.

For general estimation of the error of the X, Y coordinate measurement method, the average value of the systematic component of the error and the average value of the random error for two impact points were used (see Fig. 1). The summary values of the errors are given in Table 2, where Δ_X and Δ_Y are the average values of systematic errors in determining the X - and Y -coordinates.

As follows from Table 2, the systematic component of the error increases along with the random component. The minimum errors were obtained using an electronic simulator. Comparing the location errors of AE signals when using different calculation methods (see Table 1), it can be noted that the lowest average values of the systematic and random error components were obtained by the RMD method when dropping a ball with a diameter of $d = 10$ mm from a height of $h = 600$ mm. The greatest errors in determining the coordinates from the impact were obtained when a ball with a diameter of 16 mm was dropped onto the sample from a height of 300 mm.

The two-interval coefficient was used to estimate the measurement error of AE signal arrival time. For the planar location of AE signals when using the three-channel antenna, the channel with a minimum two-interval coefficient was selected, since it introduces the greatest error in the calculation of arrival times. The correlation of the average value of this coefficient at the impact points with the value of the random error of coordinates was calculated. This coefficient corresponds to the signal-to-noise ratio of the signal where the arrival time is determined in the time domain.

The shape of an AE signal produced by the simulator differs considerably from the shape of the signal obtained when dropping a metal ball. This is accompanied by a decrease in the amplitude of the fast mode $S0$, whose time of arrival is considered to be the signal arrival time in all considered calculation algorithms. The main differences in all methods of impact on a composite sample are the change in the ratio of the amplitudes of the fast $S0$ and slow $A0$ modes. In addition, differences are observed in the spectrum of AE signals, since the energy in the spectrum is slightly shifted towards the low-frequency region due to shock effects (Table 3).

In Table 3, $K(t)$ denotes the average value of the two-interval coefficient for all signals at the start point of the signal of the fast $S0$ mode. The signal-to-noise ratio is denoted by S/N_{s0} and S/N_{a0} and is determined by the ratio of the maximum signal span to the noise span in the past history for the fast $S0$ and

Table 2. Averaged values of systematic and random errors in determining X - and Y -coordinates for various AE signal simulators

Type of AE signal simulator	Δ_x , mm	Δ_y , mm	S_x , mm	S_y , mm
Electronic simulator	1.4 0.4%	5.2 1.9%	1.0 0.3%	1.5 0.5%
Su–Nielsen simulator	2.6 0.7%	6.4 2.3%	1.8 0.5%	1.6 0.6%
Dropping ball with diameter $d = 10$ mm from height $h = 600$ mm	2.9 0.8%	5.3 1.9%	2.6 0.7%	2.4 0.9%
Dropping ball with diameter $d = 10$ mm from height $h = 300$ mm	3.3 0.9%	5.0 1.8%	2.9 0.8%	3.7 1.3%
Dropping ball with diameter $d = 16$ mm from height $h = 600$ mm	3.2 0.9%	6.8 2.4%	3.7 1.0%	5.4 1.9%
Dropping ball with diameter $d = 16$ mm from height $h = 300$ mm	3.8 1.1%	9.5 3.4%	4.5 1.3%	6.3 2.3%

Table 3. Parameters of the shape and spectrum of AE signals received from sensor AET3 at point 6 (see Fig. 1) of sample for different types of impacts

AE signal simulator type	Two-interval coefficient $K(t)$	Signal-to-noise ratio for fast mode S/N_{s0}	Signal-to-noise ratio for slow mode S/N_{a0}	Median frequency F_{med} of spectrum, kHz	Ratio of the amplitude of the slow mode to that of the fast mode $P_{a0/s0}$
Electronic simulator	101.8	106.6	334.3	126	3.13
Su–Nielsen simulator	45.6	67.02	348.6	113	5.2
Dropping ball with diameter $d = 10$ mm from height $h = 600$ mm	10.88	44.75	400	111	8.94
Dropping ball with diameter $d = 10$ mm from height $h = 300$ mm	7.4	36.26	420	109	11.58
Dropping ball with diameter $d = 16$ mm from height $h = 600$ mm	7.55	28.26	502.2	115	17.77
Dropping ball with diameter $d = 16$ mm from height $h = 300$ mm	6.35	36.58	639.58	117	17.48

slow $A0$ modes. The median frequency of the AE signal spectrum is denoted by F_{med} , and the ratio of the amplitude of the slow mode to the amplitude of the fast mode is designated as $P_{a/s}$.

The main difference of these signals from those due to the impact with a steel ball is an increase in the ratio $P_{a/s}$ of the amplitudes of slow and fast modes (see Table 3) and a decrease in the average value of the two-interval coefficient $K(t)$.

The antenna consisting of four FOS sensors was used to estimate the error in determining the coordinates of the source. AE signals were recorded by the eight-channel module of the SCAD-16.10 AE system in which the piezoelectric AET sensors were connected to four channels and the FOS sensors to the other four channels (see Fig. 1). The process of auto-calibration of the location zone had a feature associated with the fact that the signal from the FOS sensors exceeded the selection threshold only from the nearest emitting AET sensor of the electronic simulator. At the same time, it was not possible to determine the

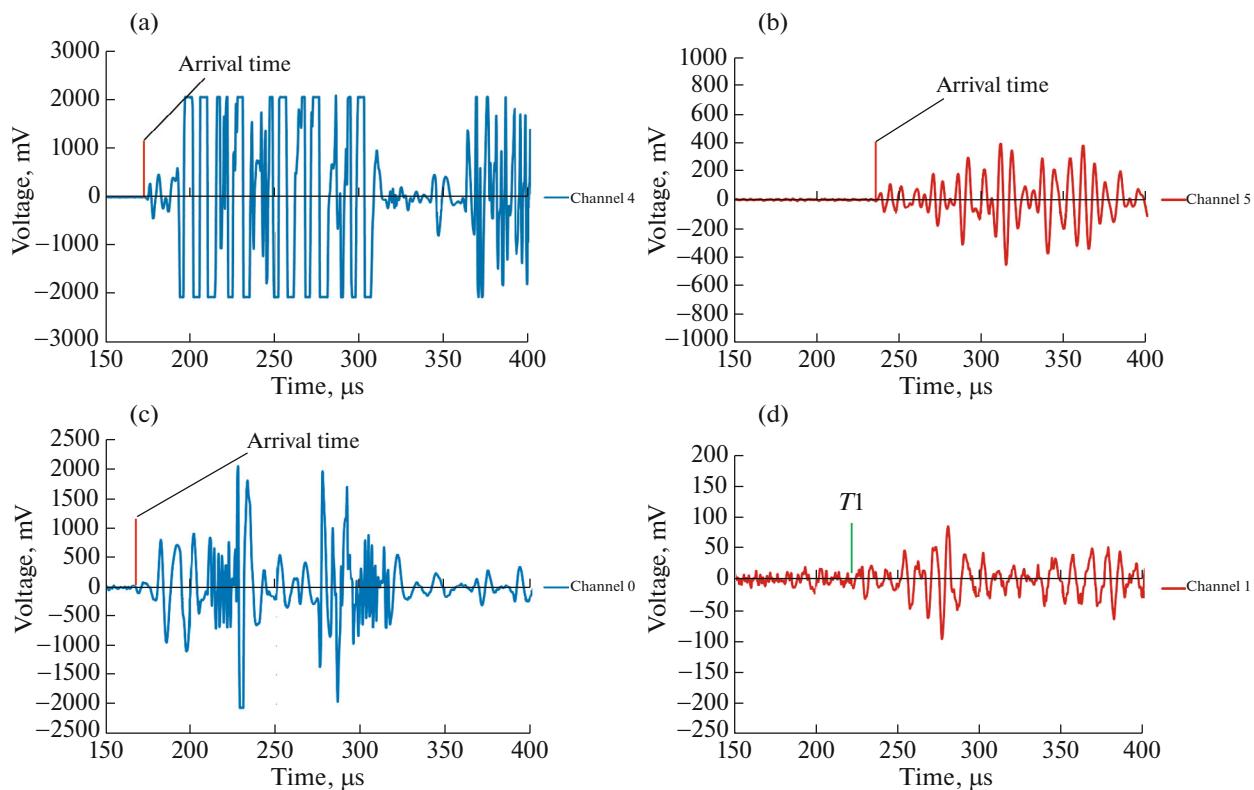


Fig. 2. Signal shape during calibration of location zone by dropping a ball with diameter 10 mm: signal at the output of sensor AET4 (a), sensor AET5 (b); signal at the output of sensor FOS0 (c), sensor FOS1 (d).

speed of sound from the FOS signals during autocalibration using electronic simulator. The speed of sound was determined during calibration using a ball dropped at a point outside the location zone on the line between the pair of FOS sensors.

Figure 2a shows the shape of an AE signal due to the ball with diameter 10 mm dropped outside the location zone between piezoelectric sensors AET4 and AET5, and Fig. 2b shows the shape of an AE signal due to this ball dropped in the area between sensors FOS0 and FOS1. The distance between these sensors was 360 mm, and the speed of a sound wave of the fast mode S_0 according to the results of the measurement of the ATD of piezoelectric sensors AET4 and AET5 was $V_x = 360 \text{ mm}/70 \mu\text{s} = 5.14 \text{ mm}/\mu\text{s}$.

The time of arrival of the AE signal to the sensor FOS0 was reliably determined (Fig. 2c). The time of arrival at sensor FOS1 was visually determined as T_1 (Fig. 2d). For the arrival time T_1 , the ATD is $62 \mu\text{s}$ and the velocity $V_x = 350 \text{ mm}/62 \mu\text{s} = 5.64 \text{ mm}/\mu\text{s}$. Calibration with FOS sensors gives a large error in determining the velocity of the fast mode S_0 , therefore, calibration results obtained by piezoelectric sensors AET4 and AET5 were used to calculate the coordinates.

The results of calculations of coordinates for the case of dropping the ball with diameter 10 mm from the height of 600 mm for location zones made up of combinations of AET and FOS sensors are shown in Table 4. In this table, location zone 1 is composed of four piezoelectric AET sensors (AET2, AET3, AET4, and AET5). Two FOS sensors and two piezoelectric AET sensors (FOS0, FOS1 and AET2, AET3) were included in location zone 2. Location zone 3 consisted of two FOS and two piezoelectric AET sensors (AET4, AET5 and FOS6, FOS7). Zone 4 consisted of four FOS sensors (FOS0, FOS1, FOS6, and FOS7). When arranging various antennas, the AET and FOS sensors on the sample did not move.

The location errors in zones 2 and 3 increase considerably when two FOS sensors are included in the antenna compared to zone 1 (see Table 4). The increase in the error in determining the coordinates is due to the low amplitude of the signals recorded by the FOS sensors caused by their low sensitivity and errors in determining the time of arrival of signals.

Table 4. Design values of systematic and random error in determining X - and Y -coordinates averaged over impact points for four location zones using AET and FOS sensors

Location zone number	Localized events, %	Δ_X , mm	Δ_Y , mm	S_X , mm	S_Y , mm
1	98.8	4.2	8.6	2.3	3.3
		1.2%	3.1%	0.6%	1.2%
2	78.1	9.7	32.3	8.9	31.7
		2.7%	11.5%	2.5%	11.3%
3	61.0	36.6	62.3	7.3	37.8
		10.5%	22.3%	2.0%	13.5%
4	53.7	64.6	68.2	44.0	56.6
		17.9%	24.4%	12.2%	20.2%

When using the antenna consisting of four AETs that form zone 1, all shock effects applied at 16 points were localized (Fig. 3a). The average location error for all points in this case was 4.2 mm on the X -axis and 8.6 mm on the Y -axis. At the same time, 98.8% of all recorded signals were localized (see Table 4).

The replacement of two AET sensors with FOS sensors led to a substantial drop in the accuracy of determining the coordinates of localized AE signals. The results of determining the coordinates of AE signals for location zones 2 (Fig. 3b) and 3 (Fig. 3c) were analyzed.

The accuracy of locating AE signals in zone 2 was higher than in zone 3 (see Table 4). The systematic component of the X -axis error in zone 2 was four times smaller than in zone 3 and amounted to 9.7 mm. Along the Y -axis, the systematic error was equal to 32.3 mm, that is, it was two times smaller than in zone 3. In addition, 18% more signals were localized in zone 2 than in zone 3 (see Fig. 3b).

Figure 3c shows the results of location when using the antenna forming zone 3. In this case, the share of localized AE signals decreased to 61% of all recorded ones, and the errors began to be 36.6 mm along the X -axis and 62.3 mm along the Y -axis (see Table 4). The maximum total amplitude of signals localized in zone 1 was twice as high as in zone 3. Thus, the inclusion of various FOS sensors in the second and third antennas (see Figs. 3b–3c) had an impact on the accuracy of location results. This is determined by the low sensitivity and the spread of characteristics of FOS sensors.

When using the antenna consisting of four FOS sensors, no location of AE signals was obtained when the steel ball weighing 18.5 g was dropped on the sample. Therefore, in order to achieve stable location of AE signals, we used a shock effect produced by a blunt tip load weighing $m = 530$ g [10]. The load was dropped from heights of $h_1 = 200$ mm and $h_2 = 400$ mm. The values of the energy of the dropped load weighing $m = 530$ g calculated using formula (1) were $E_1 = 1$ J for the drop height $h_1 = 200$ mm and $E_2 = 2$ J for the drop height $h_2 = 400$ mm. At the same time, the maximum amplitude of localized AE signals (Fig. 3d) was equal to 0.6 V. Dropping the load weighing $m = 530$ g at four points 5, 8, 10, and 11 marked on the sample (see Fig. 1) allowed obtaining the location shown in Fig. 3d.

When a shock damage was inflicted, the load was dropped from a height of $h_2 = 400$ mm. During the test, 62 AE signals were registered, with 28 of them corresponding to impacts and the rest to load bounces and noises. Filtering was performed to estimate the errors and only useful signals were selected. Table 5 shows the results of calculating systematic and random errors for points 5, 8, 10, and 11 shown in Fig. 1. The largest values of the error in determining the coordinates were obtained in the location area for an impact at point 5. The total systematic component of the error was $\Delta_{XY} = 54.3$ mm, and the total random component was $S_{XY} = 23.2$ mm. The highest accuracy was observed for an impact at point 8. In this case, the systematic and random error components were equal to $\Delta_{XY} = 9.7$ mm and $S_{XY} = 10.6$ mm.

It was noted that when processing AE information recorded by FOS sensors, a decrease in location accuracy was associated with their low sensitivity and, as a consequence, with difficulties in determining the arrival times of AE signals.

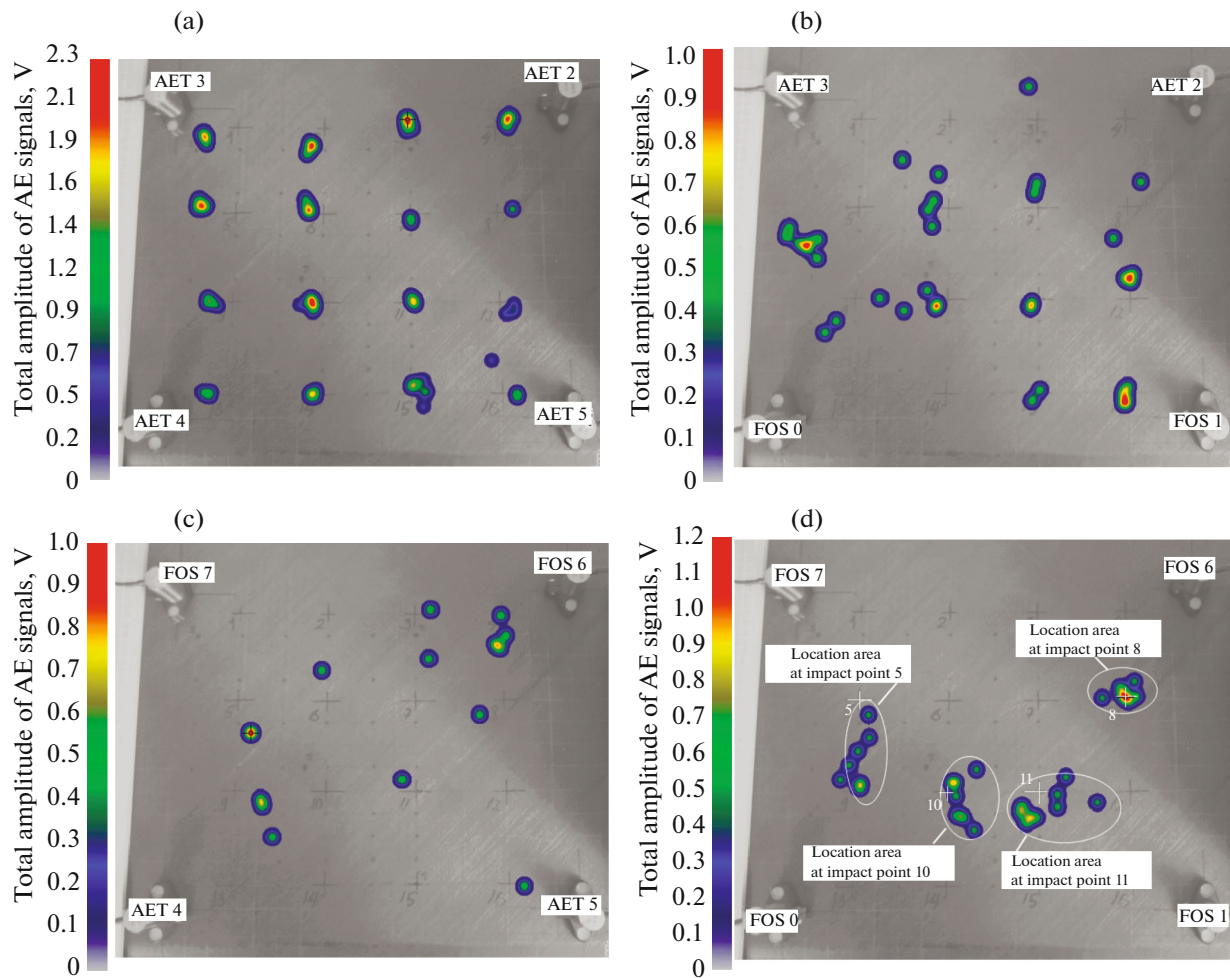


Fig. 3. Location of AE signals when using piezoelectric antennas consisting of four AETs (a), two AETs and two FOS (b, c), four FOS (d).

CONCLUSIONS

1. Methods for determining the arrival times of AE signals to antenna sensors are analyzed. It is established that the smallest location errors from impacts with a steel ball with a diameter of 10 mm dropped from a height of 600 mm are achieved by using an antenna consisting of four AETs using the RMSD method when determining the arrival times of AE signals. At the same time, the average location error was

Table 5. Design values of systematic and random error in determining X- and Y-coordinates when applying shock damage at points 5, 8, 10, and 11 of the sample and using antenna consisting of four FOS sensors

Point number (see Fig. 1)	Δ_x , mm	Δ_y , mm	S_x , mm	S_y , mm	Δ_{XY} , mm	S_{XY} , mm
5	22.3	49.5	8.1	21.7	54.9	23.2
	6.2%	17.7%	2.2%	7.8%	18.7%	8.1%
8	9.1	3.5	9.0	5.6	9.7	10.6
	2.5%	4.4%	2.3%	2.0%	2.8%	3.2%
10	23.7	1.0	7.8	17.6	23.7	19.3
	6.6%	0.3%	2.2%	6.3%	6.6%	6.7%
11	8.4	8.8	22.2	7.8	12.1	23.5
	2.3%	3.1%	6.2%	2.8%	3.9%	6.8%

4.15 mm along the X -axis and 8.6 mm along the Y -axis (see Table 4). 98.8% of all recorded signals were localized. The largest errors (see Table 2) in determining the coordinates from the impact were obtained when a ball with a diameter of 16 mm was dropped onto the sample from a height of 300 mm.

2. During the tests, all sensors were installed on the sample once, after which, through their various combinations, four location antennas were considered. This made it possible to experimentally determine the location errors when applying shock damage for four types of antennas and analyze the possibilities of their practical usage.

3. The use of an antenna consisting of two AET and two FOS sensors led to a decrease in the accuracy of determining the coordinates of localized AE signals. In this case, strikes were delivered with a ball 10 mm diameter dropped from a height of 600 mm. The share of localized AE signals decreased to 61.0% of those registered, and the errors began to be 36.6 mm along the X -axis and 62.3 mm along the Y -axis.

4. In the case of using an antenna consisting of four FOS sensors, due to their low sensitivity, the impacts caused by the balls were not localized by the AE system. Therefore, to investigate the possibilities of location, the impact energy was increased and a load weighing 530 g dropped from a height of 400 mm was used. In this case, the minimum values of systematic and random error were $\Delta_{XY} = 9.7$ mm and $S_{XY} = 10.6$ mm.

OPEN ACCESS

This article is licensed under a Creative Commons Attribution 4.0 International License, which permits use, sharing, adaptation, distribution and reproduction in any medium or format, as long as you give appropriate credit to the original author(s) and the source, provide a link to the Creative Commons license, and indicate if changes were made. The images or other third party material in this article are included in the article's Creative Commons license, unless indicated otherwise in a credit line to the material. If material is not included in the article's Creative Commons license and your intended use is not permitted by statutory regulation or exceeds the permitted use, you will need to obtain permission directly from the copyright holder. To view a copy of this license, visit <http://creativecommons.org/licenses/by/4.0/>.

REFERENCES

1. Feigenbaum, Yu.M., Mikolaichuk, Yu.A., Metelkin, E.S., and Batov, G.P., The place and role of nondestructive testing in the system of maintaining the airworthiness of composite structures, *Nauchn. Vestn. GosNIIGA*, 2015, no. 9, pp. 71–82.
2. Feigenbaum, Yu.M. and Dubinskii, S.V., Influence of accidental operational damage on the strength and life of an aircraft structure, *Nauchn. Vestn. MGTU GA*, 2013, no. 187, pp. 83–91.
3. Chernishev, S.L., Zichenkov, M.Ch., Smotrova, S.A., Novotortsev, V.M., and Muzafarov, A.M., Technology for detecting inconspicuous shock damage to power elements of aircraft structures made of polymer composite materials using shock-sensitive polymer coatings with optical properties, *Konstr. Kompoz. Mater.*, 2018, no. 4, pp. 48–53.
4. Badger, V.E., Stepanova, L.N., Chernova, V.V., and Kabanov, S.I., Location of destruction zones during strength tests of an aircraft fuselage made of carbon fiber, *Polet*, 2017, no. 2, pp. 21–26.
5. Badger, V.E., Ser'eznov, A.N., Stepanova, L.N., and Chernova, V.V., Acoustic emission control of defects in the carbon fiber wing caisson during static and shock loading, *Polet*, 2019, no. 5, pp. 17–24.
6. Madaras, E., Highlights of NASA's role in developing state-of-the-art nondestructive evaluation for composites: NASA Document ID 20050050900, *Am. Helicopter Soc. Hampton Roads Chapter Struct. Spec. Meeting*, Williamsburg, 2001.
7. Ser'eznov, A.N., Stepanova, L.N., Murav'ev, V.V., Komarov, K.L., Kareev, A.E., Kabanov, S.I., Lebedev, E.Yu., Kozhemyakin, V.L., Bobrov, A.L., Boyarkin, E.V., Murav'ev, M.V., and Becher, S.A., *Diagnostika ob'ektov transporta metodom akusticheskoi emissii* (Diagnostics of transport objects by acoustic emission method), Moscow: Mashinostroenie, 2004.
8. Ser'eznov, A.N., Stepanova, L.N., Kabanov, S.I., Ramazanov, I.S., Chernova, V.V., and Kuznetsov, A.B., Location of acoustic emission signals in duralumin and carbon fiber samples using an antenna consisting of fiber-optic sensors and piezoelectric converters, *Kontrol' Diagn.*, 2021, no. 2, pp. 18–29.
9. Stepanova, L.N., Petrova, E.S., and Chernova, V.V., Strength tests of a CFRP spar using methods of acoustic emission and tensometry, *Russ. J. Nondestr. Test.*, 2018, vol. 54, no. 4, pp. 243–248.
10. Stepanova, L.N., Chernova, V.V., and Miloserdova, M.A., Acoustic emission control of the process of destruction of samples and a carbon fiber wing caisson from shock loads, *Kontrol' Diagn.*, 2020, vol. 23, no. 9, pp. 4–11.

11. Becher, S.A. and Popkov, A.A., Time characteristics of the acoustic emission signal flow during the development of cracks in glass under shock loading, *Vestn. IzhGTU im. M.T. Kalashnikova*, 2019, vol. 22, no. 1, pp. 62–71.
12. Bochkova, S.D., Volkovskii, S.D., Efimov, M.E., Deineka, I.G., Smirnov, D.S., and Litvinov, E.V., A method for determining the locations of impacts in a composite material using fiber optical acoustic emission sensors, *Instrum. Exp. Tech.*, 2020, vol. 63, no. 4, pp. 507–510.
13. Bashkov, O.V., Zaikov, V.I., Khun, K., Bashkov, I.O., Romashko, R.V., Bezruk, M.N., and Panin, S.V., Detecting acoustic-emission signals with fiber-optic interference transducers, *Russ. J. Nondestr. Test.*, 2017, vol. 53, no. 6, pp. 415–421.
14. Fedotov, M.Yu., Budadin, O.N., and Kozel'skaya, S.O., Features of the technology of optical nondestructive testing of composite structures with fiber-optic sensors, *Konstr. Kompoz. Mater.*, 2020, no. 2, pp. 52–55.
15. Yu, F., Okabe, Y., Wu, Q., and Shigeta, N., Damage type identification based on acoustic emission detection using a fiber-optic sensor in carbon fiber reinforced plastic laminates, *32nd Eur. Conf. Acoust. Emiss. Test.* (Prague, 2016).
16. Lexmann, M., Bueter, A., and Schwarzaupf, O., Structural Health Monitoring of composite aero-space structures with Acoustic Emission, *J. Acoust. Emiss.*, 2018, vol. 35, pp. 172–193.
17. Soman, R., Wee, J., and Peters, K., Optical fiber sensors for ultrasonic structural health monitoring: A review, *Sensors*, 2021, vol. 21, no. 21, p. 7345.
<https://doi.org/10.3390/s21217345>
18. Willberry, J.O., Papaalias, M., and Fernando, G.F., Structural health monitoring using fiber optic acoustic emission sensors, *Sensors*, 2020, vol. 20, p. 6369.
<https://doi.org/10.3390/s20216369>
19. Yu, F. and Okabe, Y., Fiber-optic sensor-based remote acoustic emission measurement in a 1000°C environment, *Sensors*, 2017, vol. 17, p. 2908.
20. Tada, K. and Yuki, H., Detection of acoustic emission signals with the fabry-perot interferometer type optical fiber sensor, *J. Acoust. Emiss.*, 2017, vol. 34, pp. S38–S41.
21. Popkov, A.A. and Becher, S.A., Application of spatial correlation of parameters of acoustic emission signals for solving problems of clustering of sources, *Intell. Sist. Proizv.*, 2020, vol. 18, no. 4, pp. 30–38.
<https://doi.org/10.22213/2410-9304-2020-30-38>
22. Goncharov, A.A. and Kopilov, V.D., *Metrologiya, standartizatsiya i sertifikatsiya v stroitel'stve: uchebnoe posobie* (Metrology, Standardization, and Certification in Construction: a Textbook), Moscow: KnoRus, 2022.